FutureGen Industrial Alliance, Inc.
73 Central Park Plaza East
Jacksonville, IL 62650
www.FutureGenAlliance.org

Kenneth Humphreys
Chief Executive Officer
217-243-8215

December 10, 2013

Stephen Jann
Acting Branch Chief, Underground Injection Control Branch
United States Environmental Protection Agency – Region 5
Mailcode: WU-16J
77 West Jackson Blvd
Chicago, IL 60604-3590

Subject: Request for Additional Information #2 Regarding, FutureGen Applications for UIC Permit nos. IL-137-6A-0001, -0002, -0003 & -0004, November 14, 2013

Dear Mr. Jann,

Please find enclosed one printed copy and one compact disc with an electronic copy of the FutureGen Alliance's responses to your Request for Additional Information (RAI #2) on the FutureGen Alliance's UIC applications dated November 14, 2013.

Inquiries concerning the contents of the enclosure may be directed to Tyler Gilmore by telephone (509) 371-7171 or by email to tyler.gilmore@pnnl.gov .

Sincerely,

Mr. Kenneth Humphreys Chief
Executive Office
FutureGen Industrial Alliance, Inc.

11-14-2013: Letter from Rebecca Harvey (EPA) to Kenneth K. Humphreys (Alliance), "Request for Additional Information Regarding four FutureGen 2.0 Wells, United States Environmental Protection Agency Underground Injection Control (UIC) Permit Applications for Four Geologic Sequestration Wells; United States Environmental Protection Agency UIC Permit Nos. IL-137-6A-0001, -0002, -0003, & -0004

Requests based on the text application

RAI #	Subject	Page	Doc. Sec.	Par.	EPA Comment / Question / Request	FutureGen Response	Footnote / Reference Citation
11-14-2013_001	Physical Processes Modeled	3.3	3.1.2		"Page 3.3 of the permit application states that laboratory investigations for quantifying the importance of chemical reactions are being conducted. Are any results available? Modeling considering reactive transport may need to be conducted if the lab results indicate significant iron carbonate precipitation that changes injection zone porosity."	Based on its experiments, the FutureGen Alliance (the Alliance) expects to see a small mass of precipitates (KCl, NaCl) forming near the injection well from the $scCO_2$ displacement of water, and does not expect to see the formation of any significant carbonate precipitates in this year (or years) time scale. Iron does precipitate, but concentrations are too low (<0.6 mmol/L) relative to carbonate mass to be a precipitate issue. Simulations by others (White et al. 2005) of $scCO_2$ injection in a similar sandstone (also containing iron oxides) shows that over significantly longer time scales (1000+ years), alumino silicate dissolution and alumino silicate precipitation incorporating significant carbonate (dawsonite) is predicted, as well as precipitation of some calcite. That predicted mineral trapping did permanently sequester 21% of the carbonate mass, thus decreasing $scCO_2$ transport risk. A more detailed response to this request showing some experimental results is presented in Appendix A.	White, S.P., R. Allis, J. Moore, T. Chidsey, C. Morgan, W. Gwynn, and M. Adams. 2005. Simulation of reactive transport of injected CO_2 on the Colorado Plateau, Utah, USA. *Chemical Geology* 217:387–405.
11-14-2013_002	Intrinsic Permeability in the Injection Zone		3.1.3.2	1	"A "curve permKCal" is referenced, but the location of the curve isn't clear. Please provide a copy or further explain."	The fourth paragraph of page 3.6 of the Supporting Documentation for the Alliance's Class VI UIC permit applications (in the section "Intrinsic Permeability in the Injection Zone [Mount Simon and Elmhurst Sandstone"]) should be replaced by: *"For model layers within the injection reservoir section (i.e., Elmhurst Sandstone and Mount Simon Sandstone; 3,852 to 4,432 ft [1,174 to 1,350 m]) wireline ELAN permeability model permKCal produced by Schlumberger (red curve on Figure 2.11, page 2.17). This model, calibrated by rotary side-wall and core plug permeabilities, provides a continuous permeability estimate over the entire injection reservoir section. This calibrated permeability response was then slightly adjusted, or scaled, to match the composite results obtained from the hydrologic packer tests over uncased intervals. For injection reservoir model layers within the cased well portion of the model, no hydrologic test data are available, and permKCal values were used directly to assign average model layer permeabilities."*	
11-14-2013_003	Intrinsic Permeability in the Injection Zone		3.1.3.2	2	"No hydrologic tests were conducted in the Elmhurst formation to measure a Permeability-Thickness Product and no ELAN calculation was given. How was a Permeability-Thickness Product determined for the Elmhurst formation?"	No permeability-thickness product has been determined for the Elmhurst Formation. The permeabilities used for this formation were the ELAN-based PermKcal values without applying a scaling factor.	
11-14-2013_004	Vertical Permeability		3.1.3.2	3	"Kv/Kh measured in 20 core plug pairs; highly related to presence of mudstone/shale; sparse data led to use of literature values. Given that 20 ratios were successfully determined, how do they compare to the literature values?"	Table 3.4 of the UIC permit Supporting Documentation has been updated to show the Kv/Kh literature values for model layers that have measured values and the corresponding 20 measured Kv/Kh data points. The complete response to this request is discussed in Appendix B	
11-14-2013_005	Capillary Pressure and Saturation Functions		3.1.3.2	4	"Data was used from Manlove field to generate Brooks-Corey parameters for four different permeability ranges, shown in Table 3.5. Please provide a citation for this information."	While preparing a UIC application for the proposed Mattoon site in 2006, the State of Illinois provided the Alliance with a Data Package containing detailed information about the Mattoon site, including geological, geochemical, hydrological, tectonic, and other physical property data requested by the Alliance. The data plotted in Figure 3.12 in the current UIC application for the Morgan County site are for the Hazen #5 well in the Manlove Gas Storage Field (API#120192181400) and were provided to the Alliance by the State of Illinois as part of the Data Package. A description of the source of the geological and other data is given on page 1.1 of the Mattoon, Illinois Environmental Information Volume II[1].	[1]FutureGen Alliance. 2006. *Mattoon, Illinois Environmental Information Volume II Subsurface*. PNWD-3768, prepared for the FutureGen Alliance by Battelle - Pacific Northwest Division, Richland, Washington.
11-14-2013_006	Temperature		3.1.3.3	5	We believe 6.72^{-3} should be 6.72×10^{-3} °F/ft?	6.72^{-3} should indeed be replaced by 6.72×10^{-3} °F/ft.	
11-14-2013_007	Temperature		3.1.3.3	6	Why is regression used rather than measured data?	The temperature log does not extend to the full depth of the model domain. Therefore, a temperature gradient was calculated to use for assigning initial conditions to the model domain. A linear regression of the data (Figure 3.13) was done to best represent the trend of the temperature variation in the vertical direction. The reference temperature used in the model was chosen to be consistent with the gradient specified in the model because the discrete measured data, while within the range of uncertainty, do not directly lie on the regression line.	

11-14-2013: Letter from Rebecca Harvey (EPA) to Kenneth K. Humphreys (Alliance), "Request for Additional Information Regarding four FutureGen 2.0 Wells, United States Environmental Protection Agency Underground Injection Control (UIC) Permit Applications for Four Geologic Sequestration Wells; United States Environmental Protection Agency UIC Permit Nos. IL-137-6A-0001, -0002, -0003, & -0004

Requests based on the text application

RAI #	Subject	Page	Doc. Sec.	Par.	EPA Comment / Question / Request	FutureGen Response	Footnote / Reference Citation
11-14-2013_008	Representative Case Scenario Description	3.26	3.1.5		Section3.1.5 of the permit application notes that the design of the injection wells was chosen to "avoid sensitive areas" (p. 3.26). What are these "sensitive areas" and how were they identified? Is this the reason the horizontal well legs are not evenly distributed in a radio fashion?	The "sensitive areas" are properties to which the project has not acquired pore space rights. These properties were avoided by orienting the horizontal legs of the injection wells.	
11-14-2013_009	Computational Model Results		3.1.6	1	"It would be helpful to have a verbal description of the changes between figures in a series: e.g., the 70yr figure in 3.21 has a wide area in green but the other three do not: what does this tell us? It is extremely difficult to judge scale from these figures. Please provide dimensions of plume and pressure front over time, together. A map view, such as Fig. 3.25, would be ideal. What is the largest extent of the plume and when does this occur? Because these figures are not at the same scale, they are hard to compare."	The complete response to RAIs 11-14-2013_009 and 11-14-2013_010 is provided in Appendix C. The last paragraph and associated figures of Section 3.1.6 (Computational Model Results), beginning on page 3.29 of the Supporting Documentation of the UIC Permit applications, were updated to describe the CO_2 migration processes. The largest area of the plume is 6.46 mi^2 and occurs at year 22.	
11-14-2013_010	Computational Model Results		3.1.6	2	"Please provide figures beyond year 70. We suggest figures to year 100."		
11-14-2013_011	Parameter Sensitivity and Uncertainty		3.1.10	1	"32 cases were defined using "quasi Monte Carlo" approach. *This approach should be described and possibly cited."*	An extensive response to RAIs 11-14-2013_011 and 11-14-2013_012 is presented in Appendix D.	
11-14-2013_012	Parameter Sensitivity and Uncertainty		3.1.10	2	"The permit application states that 32 cases were defined from the representative case model. The parameter values used for these 32 cases should be presented in a table."		

11-14-2013: Letter from Rebecca Harvey (EPA) to Kenneth K. Humphreys (Alliance), "Request for Additional Information Regarding four FutureGen 2.0 Wells, United States Environmental Protection Agency Underground Injection Control (UIC) Permit Applications for Four Geologic Sequestration Wells; United States Environmental Protection Agency UIC Permit Nos. IL-137-6A-0001, -0002, -0003, & -0004

Request based on the online GS data tool modeling input

RAI #	Tab	Par.	EPA Comment / Question / Request	FutureGen Response	Footnote / Reference Citation
11-14-2013_013	Model Domain		"In the permit application and the Input Advisor submission, subsurface locations are referred to both in terms of depth (with respect to the ground surface or the Kelly bushing) and elevation (with respect to sea level). For example, the top of the open interval is described as 3,850 ft below ground surface on p. 3.26 of the permit application, while the Input Advisor submission refers to this location as having an elevation of -3,220 ft. Is it correct to assume that all of the Z coordinate values submitted in the Input Advisor represent elevations relative to sea level and are consistent (e.g., z coordinates provided for well intervals)?"	Yes, it is correct. All Z coordinate values submitted in the Input Advisor are consistent and represent elevations relative to mean sea level as used in the computational model domain. Simulation results were post-processed and converted to depth relative to Kelly Bushing (KB) at the characterization well for presentation in the UIC permit application. This was done for ease of comparison to characterization data and figures shown elsewhere in the document. The graphics provided in the Input Advisor show depth below KB (converted from the model units of elevation) to be consistent with the permit application figures. For reference: FutureGen 2.0 Stratigraphic Well (FGA#1) elevation: 633 ft (KB) / 619 ft (GS) FutureGen 2.0 Injection Well surface elevation: 630 ft	
11-14-2013_014	Rocks Properties	1	"The saturation function/relative permeability spreadsheet submitted via the Input Advisor defines the Brooks-Corey function for the relative permeability and saturation functions and provides corresponding parameters for different layers. It would be helpful if the functional forms of Brooks-Corey for the relative permeability and saturation functions were also provided in the spreadsheet."	The Brooks-Corey (1964) saturation function is given as $S_{ew} = \begin{cases} (P_e / P_c)^{\lambda} & if \quad P_c > P_e \\ 1 & otherwise \end{cases}$ where S_{ew} is effective aqueous saturation, P_c is capillary pressure, P_e is gas entry pressure, and λ is the pore-size distribution parameter. Combined with the Burdine (1953) relative permeability model, the relative permeability for the aqueous phase, krw, and that for the non-aqueous phase, krn, are $k_{rw} = (S_{ew})^{3+2/\lambda}$ $k_{rn} = (1 - S_{ew})^2 \left(1 - S_{ew}^{\,1+2/\lambda}\right)$	Brooks, R.H., and A.T. Corey. 1964. Hydraulic properties of porous media. Colorado State University Hydrology Paper No. 3. Colorado State University, Fort Collins, Colorado. Burdine, N.T. 1953. Relative permeability calculations form pore size distribution data. *Transactions of The Metallurgical Society of the American Institute of Mining, Metallurgical and Petroleum Engineers* 198:71–78.
11-14-2013_015	Rocks Properties	2	"*Horizontal intrinsic permeability of the confining zones* (see p. 3.7 of the permit application). Because of the reliability issues associated with ELAN log derived permeabilities below a certain limit (0.01 mD), FutureGen used the horizontal Klinkenberg permeabilities for each model layer. Was there any correction applied to the Klinkenberg permeabilities used for the confining zone layers, particularly because these may represent tight porous formations?"	Additional permeability corrections beyond the Klinkenberg correction were not applied. The K-Klinkenberg values were computed from K-air values, measured by Core Laboratories using an unsteady state method, using the Klinkenberg Correction Factor (KCF). The KCF values were obtained for each sample using a standard procedure (Jones 1972). An extensive discussion is presented in Appendix E.	Jones, S.C. 1972. A rapid accurate unsteady-state Klinkenberg permeameter. *Society of Petroleum Engineers Journal* 383-397.

11-14-2013: Letter from Rebecca Harvey (EPA) to Kenneth K. Humphreys (Alliance), "Request for Additional Information Regarding four FutureGen 2.0 Wells, United States Environmental Protection Agency Underground Injection Control (UIC) Permit Applications for Four Geologic Sequestration Wells; United States Environmental Protection Agency UIC Permit Nos. IL-137-6A-0001, -0002, -0003, & -0004

Request based on the online GS data tool modeling input

RAI #	Tab	Par.	EPA Comment / Question / Request	FutureGen Response	Footnote / Reference Citation
11-14-2013_016	Rocks Properties	3	"*Residual saturation.* As shown in the "Sat-function-rel-perm" spreadsheet, residual aqueous saturation values used in the FutureGen AoR model range from 0.0597 to 0.0810. Residual aqueous saturation values found in the literature for the Mt. Simon Sandstone range from approximately 0.2 to 0.4 (Zhou et al. 2010; Bandilla et al., 2012b; Krevor et al., 2012; Mathias et al., 2013). It is expected that site-specific capillary pressure and residual aqueous saturation for the FutureGen site will be generated after pre-injection testing of the proposed wells. However, an explanation of the effects of this selection on plume and pressure-front development may need to be provided."	Values for the residual aqueous saturation (S_{rw}) and the two other parameters used in the Brooks-Corey capillary pressure-saturation function (i.e. the non-wetting fluid entry pressure and a pore-size distribution parameter) were all obtained by fitting mercury (Hg) intrusion-capillary pressure data from the Manlove gas storage site in Champaign County. The fitting was applied after scaling the capillary pressures to account for the differences in interfacial tensions and contact angles for the brine-CO_2 fluid pair, relative to vapor-liquid Hg used in the measurements. The scaled data and the fits are shown in Figure 3.12. This approach has the major advantage that the three fitted parameters are consistent as they are obtained from the same original data set. The use of consistent parameter values is not the norm for brine-CO_2 flow simulations in the Mt. Simon. For instance, in the mentioned Zhou et al. (2010) paper, the non-wetting fluid entry pressure was obtained from a Leverett-J conversion of Hg data from the Frio sandstone. However, values of the pore-size distribution parameter and S_{rw} (0.25 – 0.3) are listed in their Table 1 without an explanation on how they were obtained. The S_{rw} values used in the modeling (Table 3.5) are indeed lower than the values found in the literature. The FutureGen Alliance was aware about these differences but opted to use a consistent data set for all retention parameter values instead of selecting parameter values from different data sources. An additional reason for using this approach is the considerable uncertainty in S_{rw} values for Mt. Simon rock in the literature. It was already mentioned that the source of the S_{rw} values used by Zhou et al. (2010) was not provided. Bandilla et al. (2012) states that a value of 0.3 was assumed "lacking detailed data" (Page 45). Krevor et al. (2012) used a fitted value of 0.22 (Table 2) based on a fit to pressure-saturation data with a maximum pressure of 10^7 Pa (Figure 8). Based on the shape of the Mt. Simon curve in the figure, it can be argued that a lower fitted S_{rw} value may have been obtained if data points were used for larger pressures. In general, using a lower S_{rw} value for the injection zone will possibly result in a somewhat smaller predicted CO_2 plume size and a smaller spatial extent of the pressure front compared to using a higher value of S_{rw}. Variation of S_{rw} in the confining zone (cap rock) likely has relatively little impact on CO_2 transport and pressure development owing to the typically much lower permeability of this zone relative to the underlying reservoir. It should be noted that some of the impact of the choice in S_{rw} values is relieved in the simulations by using the Webb extension (Webb, 2000) for the capillary pressure – saturation function. This extension accounts for removal of water below the imposed S_{rw} value when injected dry CO_2 dissolved part or all of the residual water.	Bandilla, K.W., M.A. Celia, T.R. Elliot, M. Person, K.M. Ellet, J.A. Rupp, C. Gable, and Y. Zhang. 2012. Modeling carbon sequestration in the Illinois Basin using a vertically-integrated approach. *Computing and Visualization in Science* 15:39-51:W02532. Krevor, S.C., R. Pini, L. Zuo, and S. M. Benson. Relative permeability and trapping of CO2 and water in sandstone rocks at reservoir conditions. Water Resources Research 48(2) Webb, S.W. 2000. A simple extension of two-phase characteristic curves to include the dry region. *Water Resources research* 36(6): 1425-1430. Zhou, Q., J.T.Birkholzer., E. Mehnert, Y.F. Lin, and K. Zhang. 2010. Modeling basin and plume-scale processes of CO_2 storage for full scale deployment. 2012. *Ground Water* 48(4): 494–514.
11-14-2013_017	Model Output		"*Surface flux.* For the flux output files, two areas (4 mi x 4 mi and 8 mi x 8 mi) were selected and fluxes were defined across the east, west, north, and south boundaries of both of those areas, as well as the top of the Franconia and the top of the Proviso. What are the i, j, k indexes that define the 4mi x 4 mi and 8mil x 8 mil areas?"	For the 4-mi x 4-mi area side surface, both the I index (easting) and J index (northing) range between 19 and 107; the K index (vertical) ranges between 1 and 51. For the 8-mi x 8-mi area, both the I index (easting) and J index (northing) range between 13 and 113; the K index (vertical) ranges between 1 and 51. For the top surfaces, K = 51 for Franconia top and 43 for Proviso top.	

11-14-2013: Letter from Rebecca Harvey (EPA) to Kenneth K. Humphreys (Alliance), "Request for Additional Information Regarding four FutureGen 2.0 Wells, United States Environmental Protection Agency Underground Injection Control (UIC) Permit Applications for Four Geologic Sequestration Wells; United States Environmental Protection Agency UIC Permit Nos. IL-137-6A-0001, -0002, -0003, & -0004

Request based on the online GS data tool modeling input

RAI #	Tab	Par.	EPA Comment / Question / Request	FutureGen Response	Footnote / Reference Citation
11-14-2013_018	AoR Pressure Front Delineation	1	"*Critical pressure calculation*. As mentioned in the previous Request for Additional Information from EPA, it is recommended that FutureGen explores alternative methods as well for the critical pressure determination, such as those described by Nicot et al. (2008); Birkholzer et al. (2011); or Bandilla et al. (2012)."	The FutureGen Alliance is assessing alternative methods based on Birkholzer et al. (2011) and Cihan et al. (2011 and 2013). These methods are discussed in Appendix F. This discussion is based on the fact that a static critical threshold pressure determination for brine flow up an open conduit or damaged borehole may not be applicable for cases where permeable units exist between the injection reservoir and lowermost underground source of drinking water (USDW) because the open conduit approach does not account for lateral flow outside the conduit or casing and into these permeable zones. At the FutureGen site there are many potential thief zones between the injection reservoir (Mt. Simon Sandstone and Elmhurst) and the lowermost USDW (St. Peter Sandstone) that could justify the use of the proposed analysis. The results of the analysis will be prepared in January 2014 describing the model, input parameters, and results of this analysis.	Birkholzer, J.T., J.P. Nicot, C.M. Oldenburg, Q. Zhou, D. Kraemer, and K.W. Bandilla. 2011. Brine Flow up a Borehole Caused by Pressure Perturbation from CO_2 Storage: Static and Dynamic Evaluations. *International Journal of Greenhouse Gas Control* 5(4):850–861. Cihan A., Q. Zhou, and J-T. Birkholzer. 2011. Analytical solutions for pressure perturbation and fluid leakage through aquitards and wells in multilayered-aquifer systems. *Water Resources Research* 47. Cihan A., J-T. Birkholzer, and Q. Zhou. 2013. Pressure Buildup and Brine Migration During CO_2 Storage in Multilayered Aquifers. *Groundwater* 51(2).
11-14-2013_019	AoR Pressure Front Delineation	2	"*Pressure differential/simulation time*. Despite not calculating a critical pressure with respect to the lowermost USDW, FutureGen did apply a pressure differential of 31.45 psi to determine simulation times – this value is described as "the pressure differential needed to force fluids from the injection zone into the surficial alluvial aquifer system through a hypothetical conduit" (p. 3.25). In other words, it was not calculated with respect to the lowermost USDW, but rather the aquifer currently in use as a drinking water source. The footprint of this pressure front indicates a larger area that may be impacted by injection compared to the footprint of the separate-phase plume. FutureGen acknowledged this pressure effect when identifying artificial penetrations and evaluated two wells that penetrate the Mt. Simon outside of the delineated AoR, about 16 mi south-southwest of the proposed storage site, nothing "Although these wells are well outside the AoR, they are within the region where increased pressures in the injection zone was expected and were therefore considered for additional review" (p.3.43). What calculations were used to determine this value of 31.45 psi?"	The pressure differential between the glacial aquifer and the injection zone discussed in this section was only used to estimate the simulation time duration and was not used for pressure front Area of Review (AoR) determination because, as mentioned in the EPA's RAI11-14-2013_019, the lowermost USDW at the FutureGen site is the St. Peter Sandstone. The 31.45 psi pressure differential between the glacial aquifer and the injection reservoir was calculated from the difference between the ambient reservoir pressure and the pressure front from Equation 4 of the EPA Draft Guidance (2011, page 35) using extrapolated pressures to the top of the Elmhurst based on Modular Dynamic Tester (MDT) tool and packer pressure measurements in the Mt. Simon (see Figure 2.29 in the UIC Permit). The details of this calculation are provided in Appendix G. As discussed on page 3.1 in of the Supporting Documentation of UIC permit applications, the reservoir pressure is above the threshold pressure calculated for the St. Peter prior to injection using the EPA Guidance method (EPA 2011) so that method could not be used for AoR determination of the pressure front. Additionally, Birkholzer et al. (2011) states that the EPA static pressure calculation may not be suitable for sites with permeable units (i.e., potential thief zones) between the injection zone and the lowermost USDW, as is the case with the FutureGen site. The response to EPA's RAI 11-14-2013_18 provides a discussion of the additional analysis being conducted to assess the impact of pressure differential causing brine flow up abandoned or poorly constructed wells.	Birkholzer, J.T., J.P. Nicot, C.M. Oldenburg, Q. Zhou, S. Kraemer, and K.W. Bandilla. 2011. Brine Flow up a Borehole Caused by Pressure Perturbation from CO_2 Storage: Static and Dynamic Evaluations. *International Journal of Greenhouse Gas Control* 5(4):850–861 EPA (U.S. Environmental Protection Agency). 2011. *Draft Underground Injection Control (UIC) Program Class VI Well Area of Review Evaluation and Corrective Action Guidance for Owners and Operators*. EPA 816-D-10-007, EPA Office of Water, Washington, D.C.
11-14-2013_020	AoR Pressure Front Delineation	3	"Temperature in St. Peter (USDW). Is 73°F, determined at the subsea elevation of 1,129 ft, measured at the stratigraphic well (API#12-137-22132-00)? This value does not match the resulting temperature for this elevation based on the linear-regression relationship given in Figure 3.13 – which indicated a temperature of about 82°F at a depth of 1,762.96 ft bKb (-1,129 ft subsea elevation)."	The actual temperature at 1,763 ft bkb is 82.65°F based on the static flowmeter survey. The value of 73°F was measured using the MDT tool just after the drilling of the well and thus does not represent the temperature of the formation at equilibrium.	

This page intentionally left blank

Appendix A

RAI 11-14-2013_001

Additional Information Regarding

Physical Processes Modeled

and

Reactive Reaction

The FutureGen Alliance (the Alliance) has experimentally investigated a number of geochemical, microbial, and physical processes related to supercritical carbon dioxide ($scCO_2$) injection into the upper Mount Simon Sandstone, which do show some precipitation at high $scCO_2$ concentrations. Over the long term (1,000s of years or longer), simulations by others show that $scCO_2$ storage as precipitates is expected to be a dominant process (Gaus et al. 2008, in Fig 2; White et al. 2005, simulation in sandstone with shale cap rock), where 20 to 50% of the carbon mass is permanently sequestered as a mineral.

The experiments were conducted at different brine/scCO2 ratios (0% to 98% $scCO_2$) in Mount Simon Sandstone, Eau Claire shale, and St. Peter Sandstone formations for the purpose of characterizing a) changes in water quality, and b) significant phase changes (i.e., precipitates) that may affect further injection. NaCl and KCl precipitates were observed forming at high $scCO_2$/brine ratios (Figure 1b) over time, as water partitions into the $scCO_2$, leaving ions behind that eventually precipitate (i.e., "salting out"). This is most likely to occur near injection wells. Major ion changes over the year (Figure 1a) are generally small, with only Na^+ and K^+ increase with 98% $scCO_2$ (with a corresponding increase in Cl^- [not shown]). Iron is observed to precipitate at nearly all $scCO_2$/brine ratios, but given the initial iron concentration of 0.6 mmol/L, the formation of siderite [$Fe(II)CO_3$] is expected only to be a relatively minor precipitate, and was not observed in the microprobe analysis of the $scCO_2$-treated Mount Simon samples. There were indications of mineral dissolution, with increasing Mg^{2+}, K^+, and SO_4^{2-} concentrations (10s to 100s of mmol/L) and a minor increase in silica. In the White et al. (2005) simulations, as the pH increased from 3.8 (acidic due to the $scCO_2$) to 4.8 over 105 years, the major mineral precipitates formed were aluminosilicates kaolinite [$Al_2Si_2O_5(OH)_4$] and dawsonite [$NaAlCO_3(OH)_2$], with a small increase in calcite precipitation, with corresponding dissolution of aluminosilicates albite [$NaAlSi_3O_8$], anorthite [$CaAl_2Si_2O_8$], and K feldspar [$KAlSi_3O_8$].

Therefore, the Alliance expects to see a small mass of precipitates (KCl, NaCl) forming near the injection well from the $scCO_2$ displacement of water, and does not expect to see the formation of any significant carbonate precipitates in this year (or years) time scale. Iron does precipitate, but concentrations are too low (<0.6 mmol/L) relative to carbonate to be a precipitate issue. Modeling by others (White et al.2005) in a similar sandstone (also containing iron oxides) shows that over significantly longer time scales (1,000+ years) significant aluminosilicate dissolution and aluminosilicate precipitation incorporating significant carbonate (dawsonite) is predicted, as well as some precipitation of calcite. That predicted mineral trapping did permanently sequester 21% of the carbonate mass, thus decreasing $scCO_2$ transport risk.

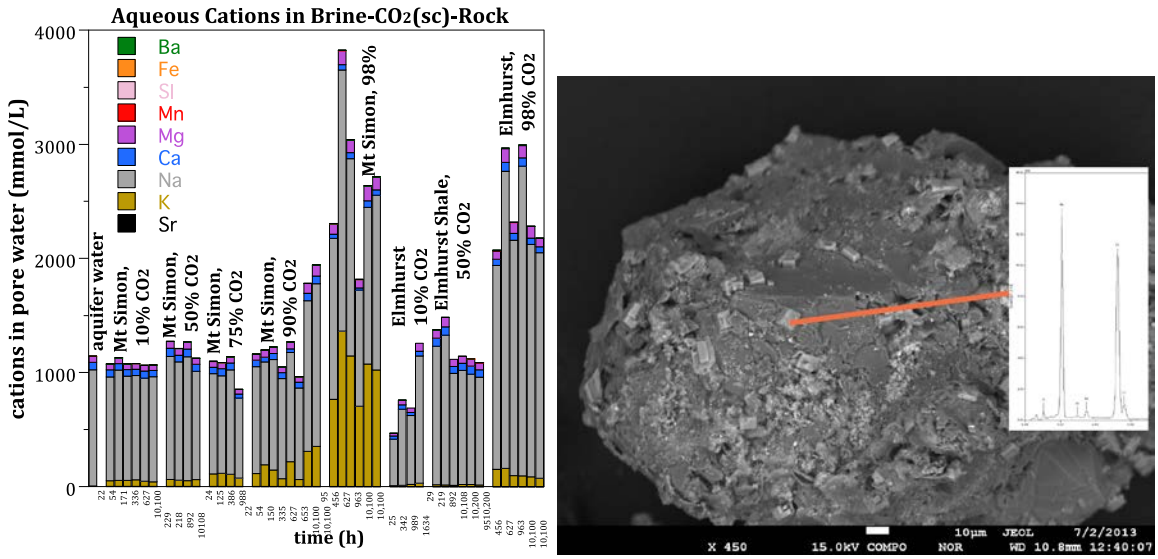

Figure 1. a) Major cation changes in Mount Simon or Elmhurst formations differing CO_2/brine mixtures over time (x-axis). Groupings are different percentages of $scCO_2$, with balance brine (i.e., 10% CO_2 is 90% brine); b) electron microprobe image of a Mount Simon Sandstone after year-long treatment with 98% $scCO_2$ showing NaCl precipitates (cubic crystals on surface).

References

Gaus, I., P. Audigane, A. Laurent, J. Lions, N. Jacquemet, P. Durst, I. Czernichowski-Lauriol, and M. Azaroual. 2008. Geochemical and solute transport modelling for CO_2 storage, what to expect from it? *International Journal of Greenhouse Gas Control* 2:605–625.

White, S.P., R. Allis, J. Moore, T. Chidsey, C. Morgan, W. Gwynn, and M. Adams. 2005. Simulation of reactive transport of injected CO_2 on the Colorado Plateau, Utah, USA. *Chemical Geology* 217:387–405.

Appendix B

RAI 11-14-2013_004

Additional Information Regarding

Vertical Permeability

The following updated Table 3.4 shows the Kv/Kh literature values for model layers that have measured values and the corresponding 20 measured Kv/Kh data points.

For the Lombard layers, core data are available for 6 of the 7 layers, with a total of 12 samples successfully analyzed for the Lombard. Of these, Kv/Kh ratios for five out of six layers are lower than the literature value; one core derived value matches the literature value of 0.1, and no core-derived Kv/Kh values exceed the literature based value.

For the Elmhurst, there are a total of four samples successfully analyzed, one each in four of the seven Elmhurst layers. Of these four samples, three have lower values than the literature value; one core-based value (Elmhurst Layer 4, sample depth 3,889–3,890 ft, Kv/Kh = 0.902) was higher than the literature value of .4.

Four Kv/Kh sample pairs were successfully analyzed in the Mount Simon cored intervals. Two samples are in Mount Simon Layer 17; two samples are from Layer 13. The geometric mean for the two samples from Layer 17 is 0.233, which is lower than the literature value of 0.4. The geometric mean of the two ratios from Layer 13 is 0.643; which is higher than the literature value.

It should be noted that there is no available whole core from the confining layers; and available rotary sidewall cores do not provide sufficient sample size for vertical measurements of permeability. The Lombard is extremely heterolithic, as observed in the attached core photos (Figure 1), but the sparse individual sample pairs suggest that the literature value represents a very conservative value, and that vertical permeability is lower than modeled.

Both Elmhurst and Mount Simon are reservoir intervals. The sparse Elmhurst and Mount Simon data generally indicate less vertical permeability than the data used in the model. While this is likely valid for the Elmhurst and uppermost Mount Simon, it should be noted that whole core data are not available for the proposed injection zone, and Kv/Kh ratios are unknown for that interval. Current characterization plans for the upcoming vertical pilot well include whole core from the injection zone and additional whole core from the Elmhurst and Mount Simon reservoirs, as well as from the Proviso and other confining zones.

Updated Table 3.4 of theSupporting Documentation for the Alliance's Class VI UIC permit application

Model Layer	Kv/Kh Applied to Model Layers[1]*	[2]Kv/Kh Determined from Core Pairs	Successfully Analyzed Core Pairs
Franconia carbonate	0.007	ND	ND
Davis-Ironton	0.1	ND	ND
Ironton-Galesville	0.4	ND	ND
Proviso (Layers 4 and 5)	0.1	ND	ND
Proviso ([carbonate] Layers 1 to 3)	0.007	ND	ND
Lombard Total Interval	0.1	0.029	12
Lombard (Layer 7)	0.1	.098	2
Lombard (Layer 6)	0.1	0.003	2
Lombard (Layer 5)	0.1	ND	ND
Lombard (Layer 4)	0.1	0.016	2
Lombard (Layer 3)	0.1	0.064	2
Lombard (Layer 2)	0.1	0.009	1
Lombard (Layer 1)	0.1	0.104	3
Elmhurst Total Interval	0.4	0.06	4
Elmhurst (Layer 7)	0.4	ND	ND
Elmhurst (Layer 6)	0.4	0.023	1
Elmhurst (Layer 5)	0.4	ND	ND
Elmhurst (Layer 4)	0.4	0.902	1
Elmhurst (Layer 3)	0.4	ND	ND
Elmhurst (Layer 2)	0.4	0.022	1
Elmhurst (Layer 1)	0.4	0.037	1
Mt. Simon (Layer 17)	0.4	0.233	2
Mt. Simon (Layer 16)	0.1	ND	ND
Mt. Simon (layer 13)	0.4	0.643	2
Mt. Simon (Layers 12, 14, and 15)	0.4	ND	ND
Mt. Simon (Layer 11, Injection)	0.5	ND	ND
Mt. Simon (Layers 6, 7, 8, 9, 10)	0.3	ND	ND
Mt. Simon (Layers 1, 2, 3, 4, 5)	0.1	ND	ND

[1] Value from literature, referenced in the Supporting Documentation of the UIC permit application
[2] Geometric mean of successful core pairs.

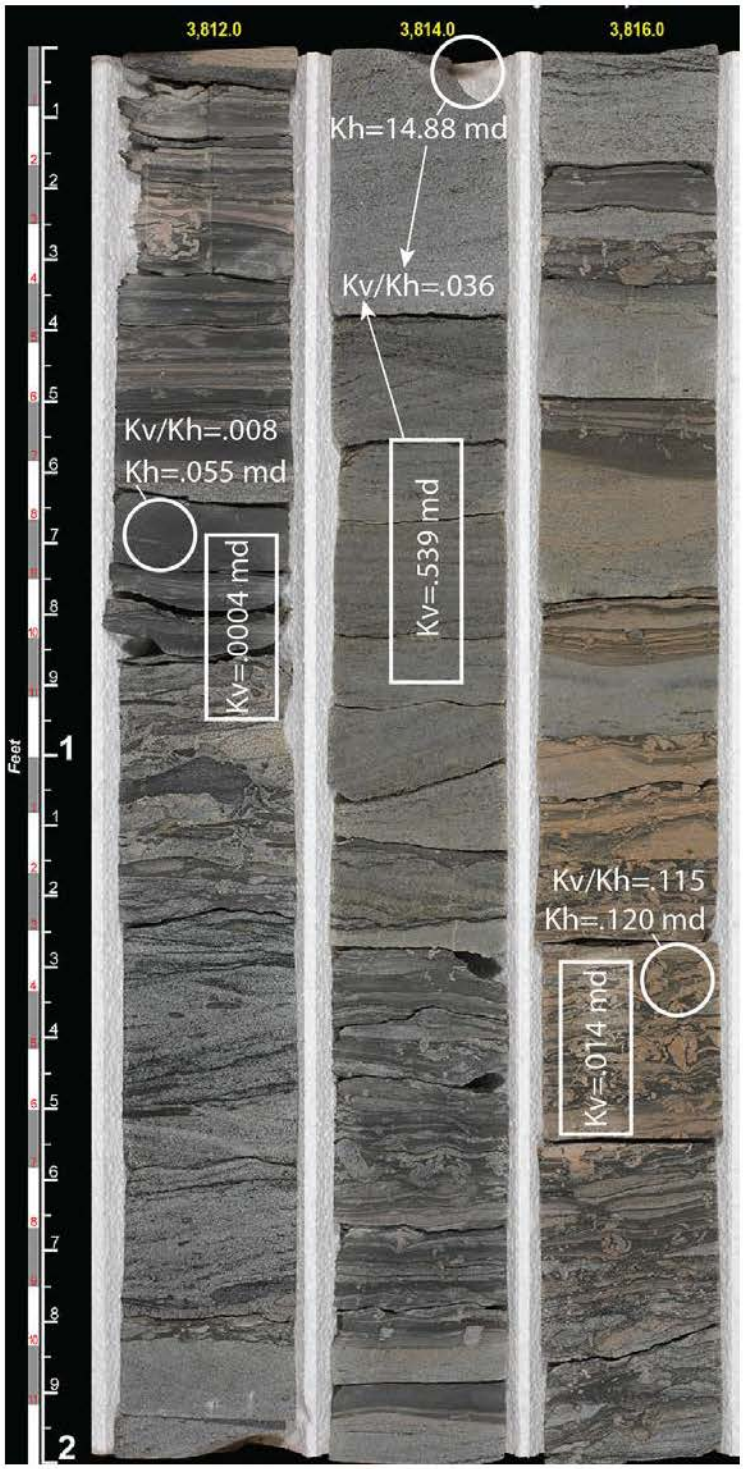

Figure 1. Slabbed core photos of the Lombard, illustrating the heterolithic nature of this interval.

Appendix C

RAI 14-11-2013_009
&
RAI 14-11-2013_010

Additional Information Regarding

Computational Model Results

The last paragraph and associated figures of Section 3.1.6 (Computational Model Results), beginning on page 3.29, were updated (as excerpted below) to describe the CO_2 migration processes. In addition, a plot corresponding to 100 years was added to each of the following figures: 3.21, 3.22, and 3.23. Furthermore, Figure 3.24 was replaced with plots showing the pressure differential and the CO_2 plume boundary at the same scale and in the horizontal plane (map view) for the same times. For convenience, the plots in each figure are marked with letters "a" through "e." Please refer to the response to RAI# 11-14-2013_018 for information about the pressure front.

"*Reservoir conditions are such that the CO_2 remains in the supercritical state throughout the domain and for the entire simulation period. The three-dimensional distribution of the CO_2-rich (or separate-) phase saturation is presented for selected times (i.e., 5, 10, 20, 70, and 100 years) in Figure 3.21. Additionally, and to better illustrate the CO_2 migration through time and space, a cross-sectional view of the CO_2 plume is presented as slices through the center of the injection wells and along the well traces (see Figure 3.18 for location of cross sections). Figure 3.22 and Figure 3.23 show the CO_2-rich (or separate) phase saturation for selected times for slices A-A' and B-B', respectively. Note that Figure 3.21 shows the plume in model coordinate space, while Figure 3.22 and Figure 3.23 show the distance from the center of the injection well pad. This is necessary because the well orientation is not aligned with the x and y axes of the model domain.*

The cloverleaf pattern of the CO_2 plume that forms as a result of the four lateral-injection-well design can be seen in Figure 3.21a, which shows the plume after 5 years of continuous CO_2 injection. The central portion of the plume is a result of CO_2 injection into the Elmhurst in the vertical section of each well. Figures presenting the cross-sectional views show the location of the open interval relative to the plume and stratigraphic units. It can be seen in Figure 3.22 and Figure 3.23 that after 5 years of continuous CO_2 injection, the plume has spread both laterally and vertically, with some CO_2 migrating into the lower part of the Lombard. At 10 and 20 years, with more CO_2 being injected, the plume grows larger with time primarily in the lateral direction, but also vertically. Two years after the cessation of CO_2 injection (at 22 years), the plume reaches its maximum lateral extent (a comparison of the plume outline at different times in plan view is shown in Figure 5.1). However, the CO_2 within the plume continues to redistribute by migrating slowly upward due to buoyancy effects, with some of the CO_2 dissolving at the CO_2-brine interface at the edge of the plume. The vertical layering represented in the model is one of the controlling factors in the plume shape at later times. In general, the CO_2 tends to accumulate below a layer with a relatively higher gas entry pressure (and often lower permeability) than that of the layer directly below it. This area of relatively higher CO_2 saturation can be seen in Figure 3.21d and Figure 3.21e as the green "ledge" feature in the plume, and in Figure 3.22d, Figure 3.22e, Figure 3.23d, and Figure 3.23e as the flat-topped orange zone. Because the plume migrates primarily upward after injection ceases, the green feature becomes narrower with time (Figure 3.21d and Figure 3.21e). The vertical cross sections showing the plume at 100 years illustrate how the CO_2 distribution within the plume becomes more uniform with time (Figure 3.22e and Figure 3.23e). Because of the dissolution process, the CO_2 separate-phase plume area (in the horizontal plane) at 100 years is 2.2% smaller than the maximum area at 22 years.

In summary, the plume grows both laterally and vertically during the injection period. Most of the CO_2 resides in the Mount Simon Sandstone. A small amount of CO_2 enters the Elmhurst and the lower part of the primary confining zone (Lombard). When injection ceases at 20 years, the lateral growth becomes negligible but the plume continues to move, primarily upward. Once CO_2 reaches the low-permeability zone in the upper Mount Simon it begins to move laterally again but at a slower rate than during injection. There is no additional CO_2 entering the confining zone from the injection zone after injection ceases.

A contour map of the pressure differential and the corresponding outline of the CO_2 plume boundary for selected times (i.e., 5, 10, 20, 70, and 100 years) are shown in Figure 3.24. The maximum pressure differential corresponds to the end of the injection period (year 20). After that time, the pressure slowly dissipates resulting in the maximum pressure differential being below 30 psi at 70 years (Figure 3.24d), and below 20 psi at 100 years (Figure 3.24e). Because there is a natural upward flow from the injection zone, a critical pressure has not been defined. Hence, we are presenting the pressure differential distribution instead of a defined pressure front (Figure 3.24).

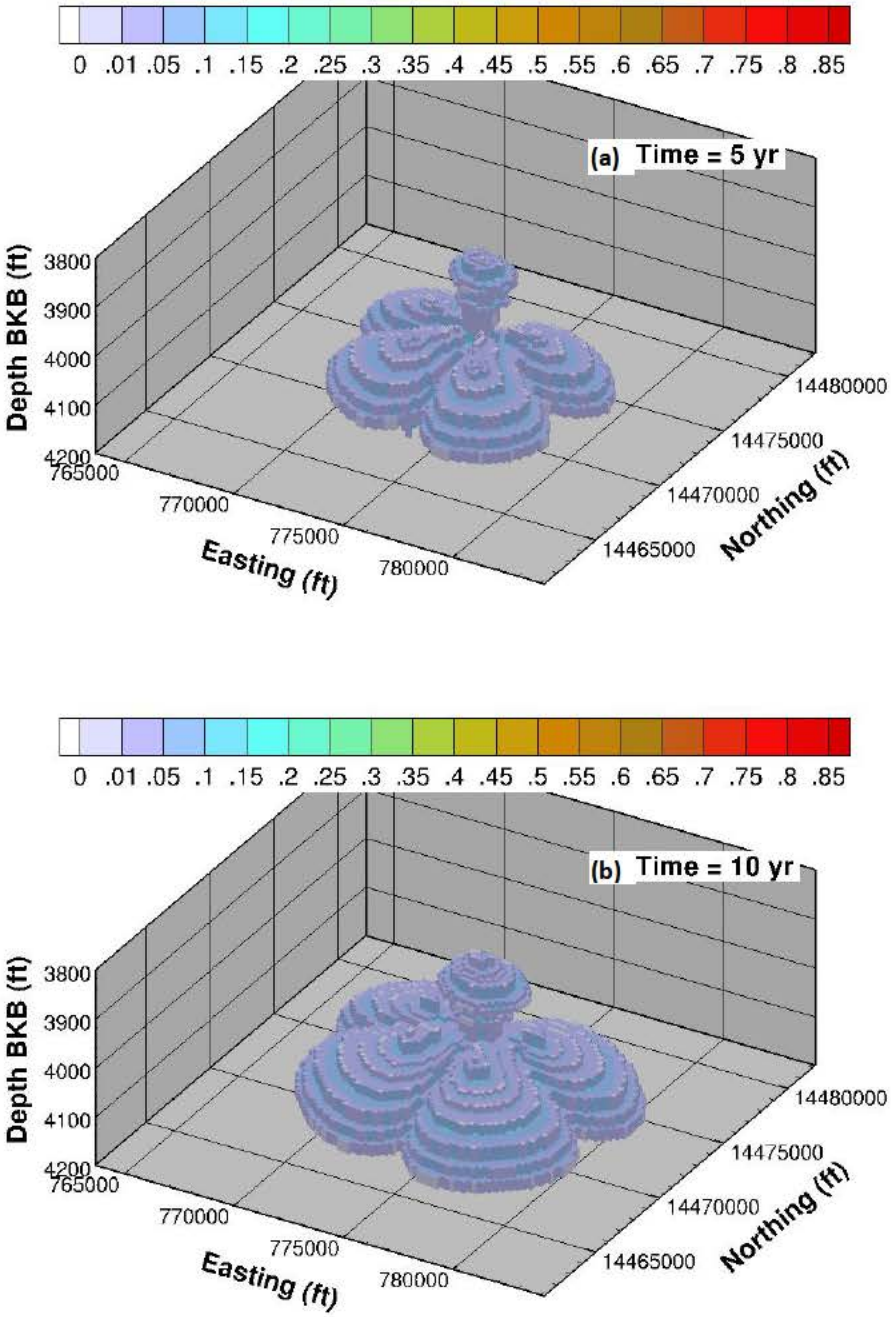

Figure 3.21. CO_2-Rich Phase Saturation for the Representative Case Scenario Simulations Shown at Selected Times (5, 10, 20, 70, and 100 years).

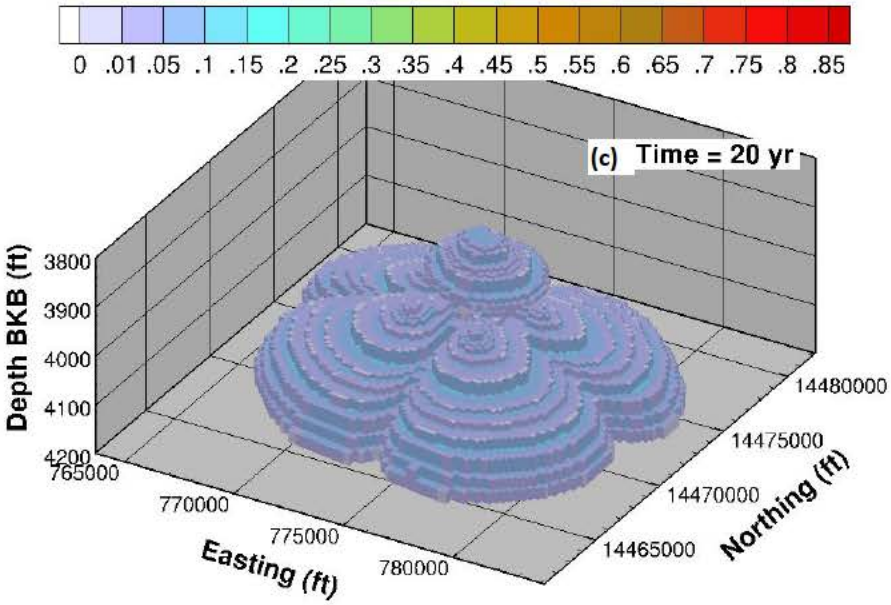

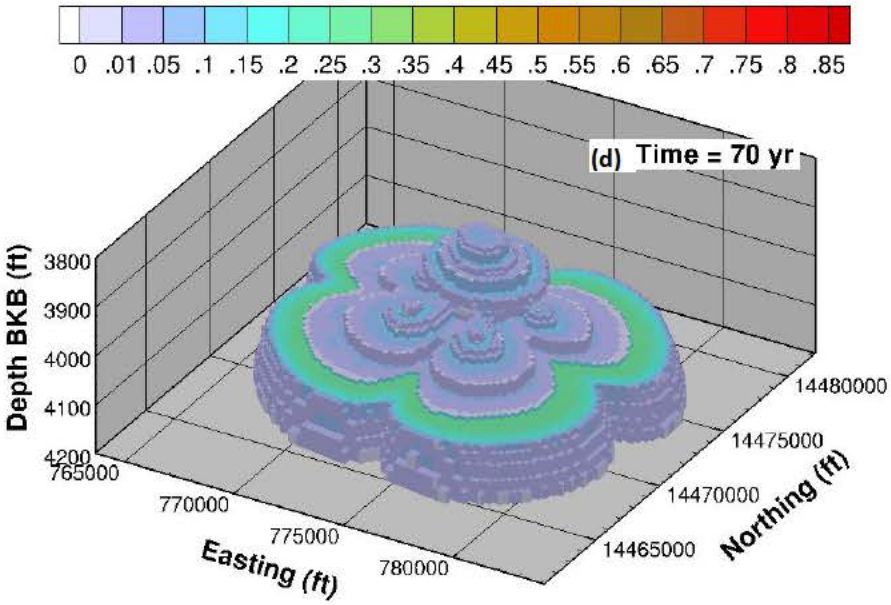

Figure 3.21. (contd)

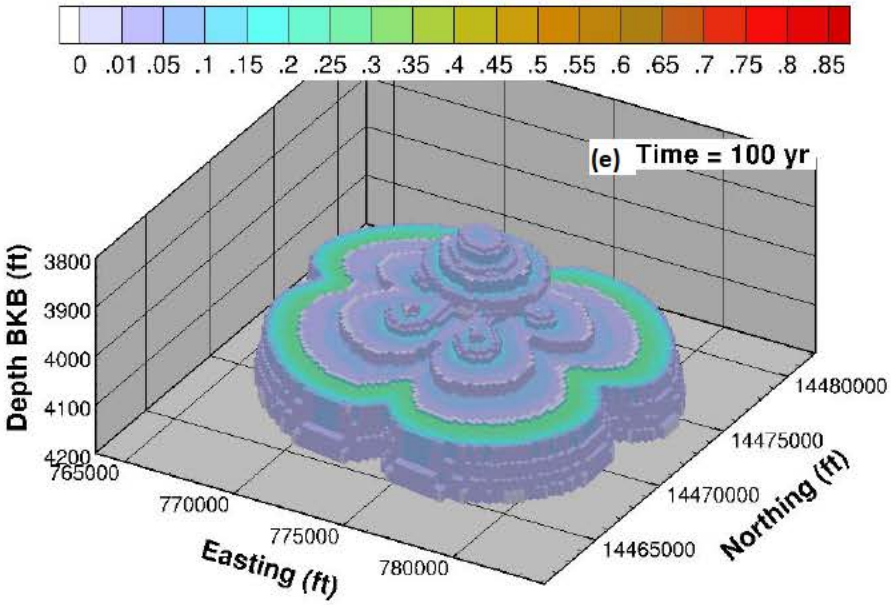

Figure 3.21. (contd)

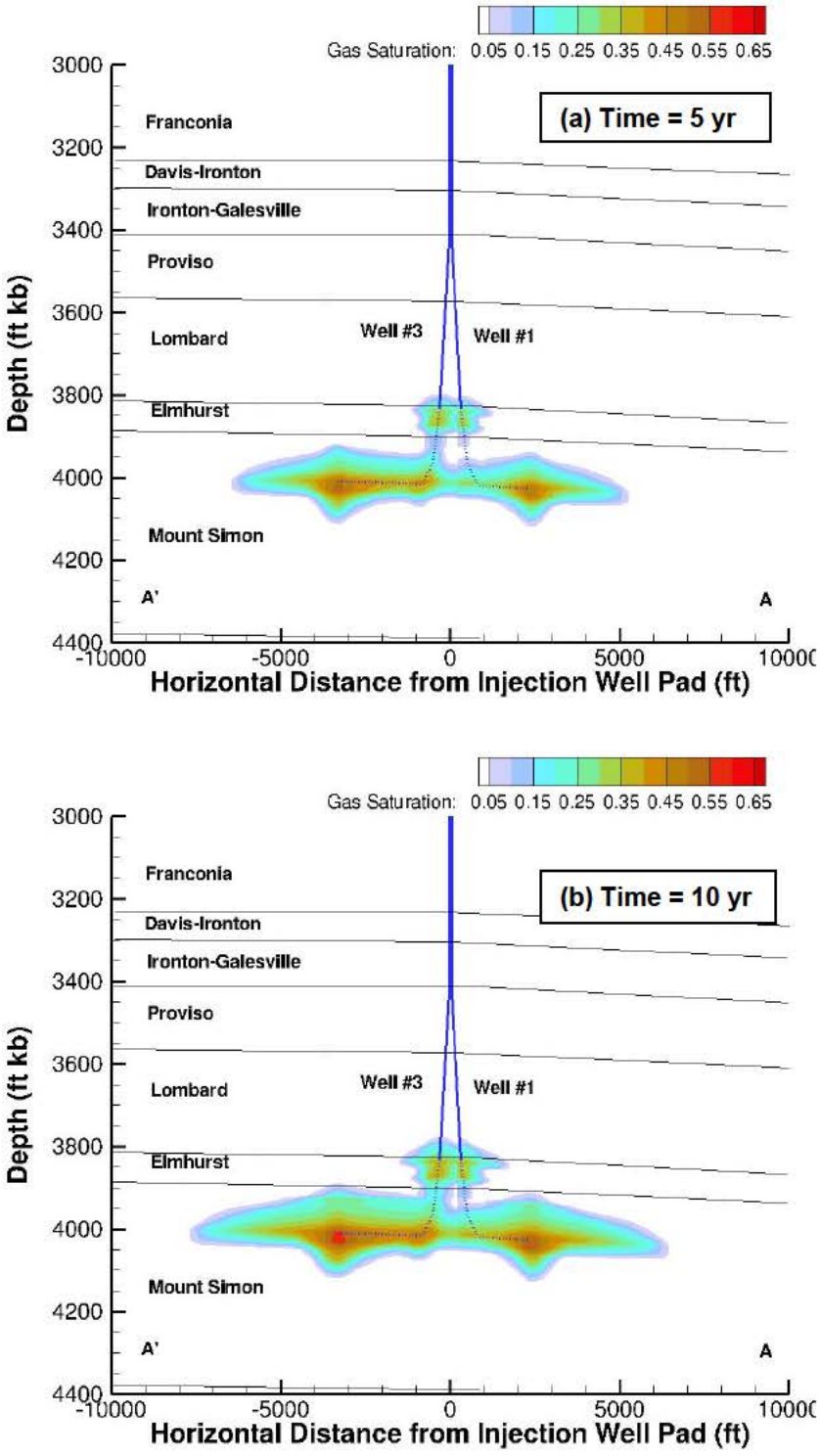

Figure 3.22. Cutaway View of CO_2-Rich Phase Saturation Along A-A' (Wells 1 and 3) for Selected Times (5 Years, 10 Years, 20 Years, and 70 Years). The dashed lines indicate open intervals of injection wells.

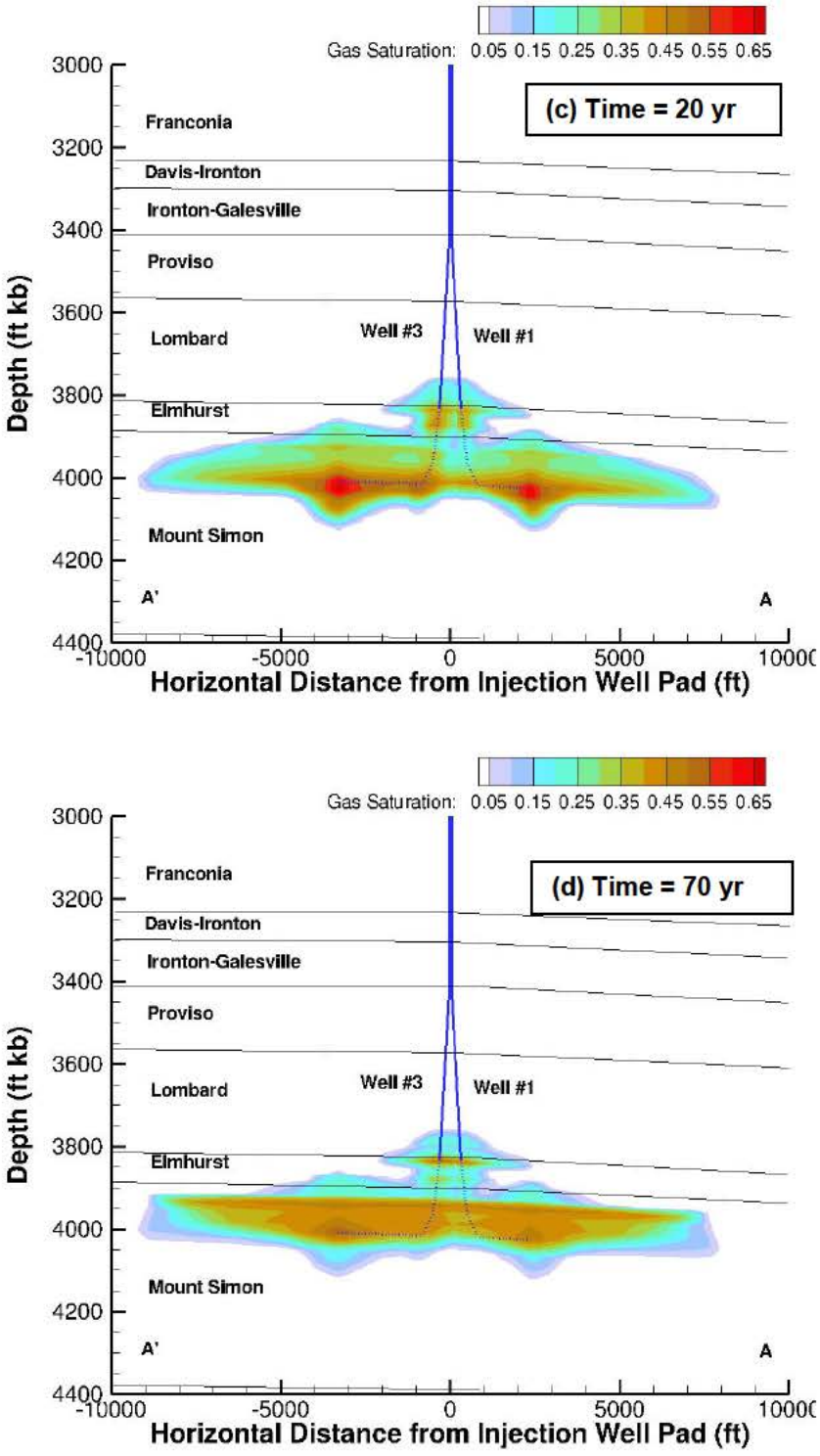

Figure 3.22. (contd)

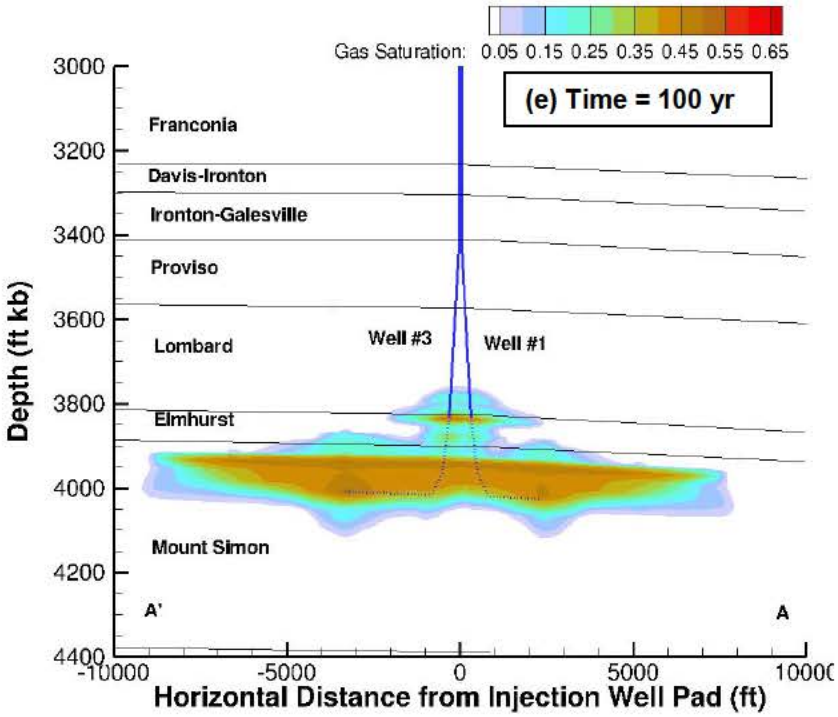

Figure 3.22. (contd)

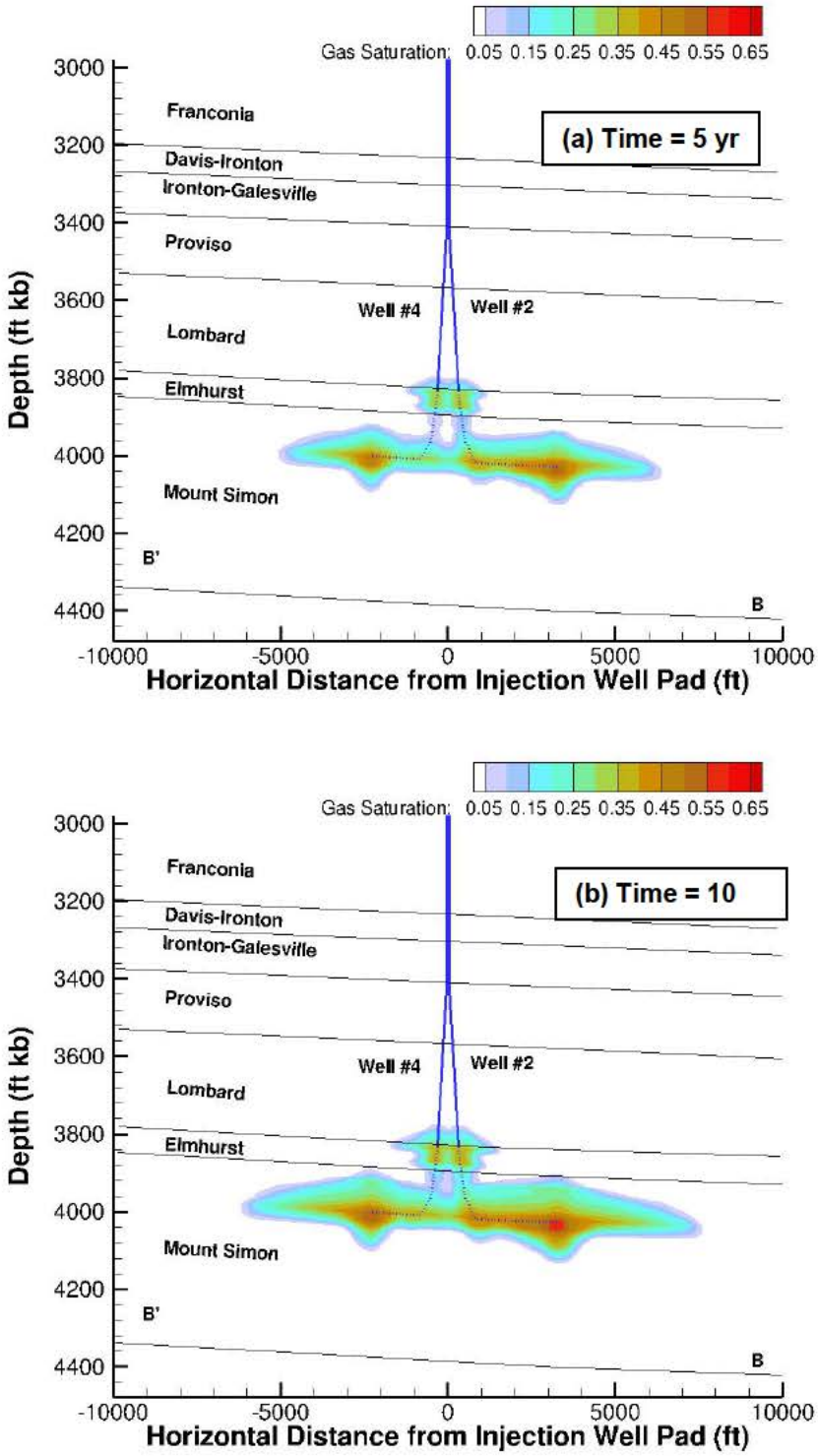

Figure 3.23. Cutaway View CO_2-Rich Phase Saturation Along B-B' (Wells 2 and 4) for Selected Times (5 Years, 10 Years, 20 Years, and 70 Years). The dashed lines indicate open intervals of injection wells.

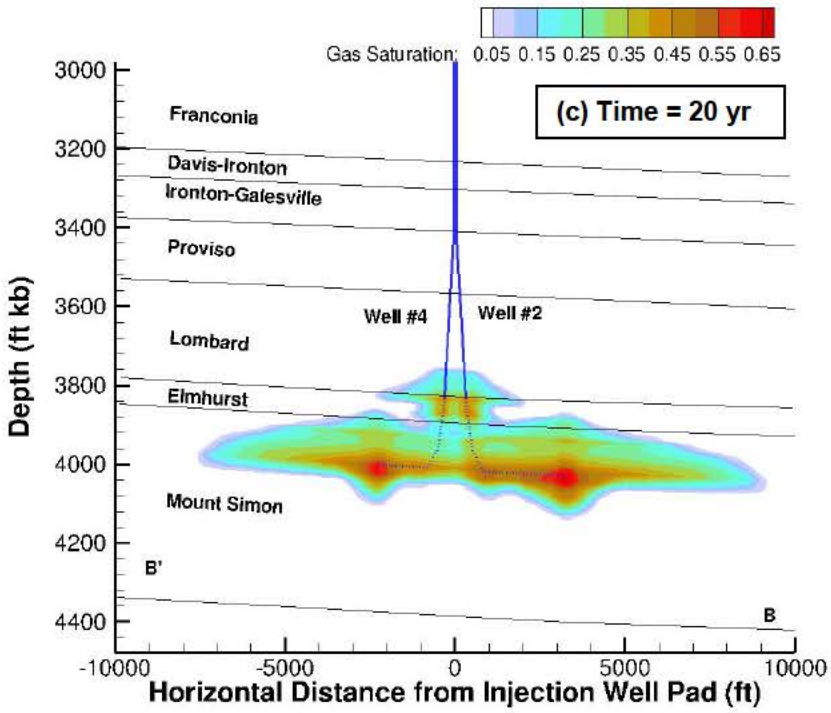

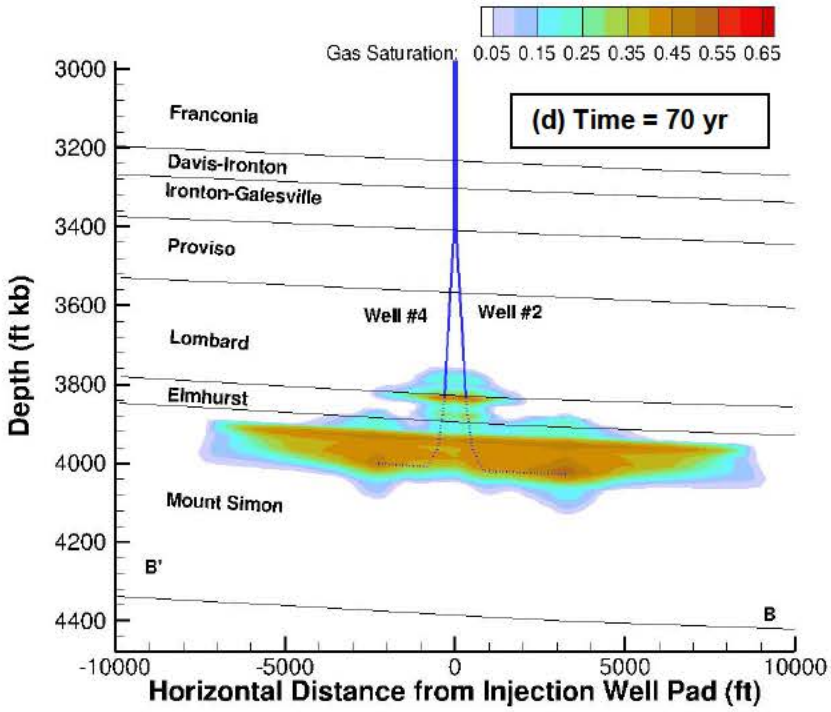

Figure 3.23. (contd)

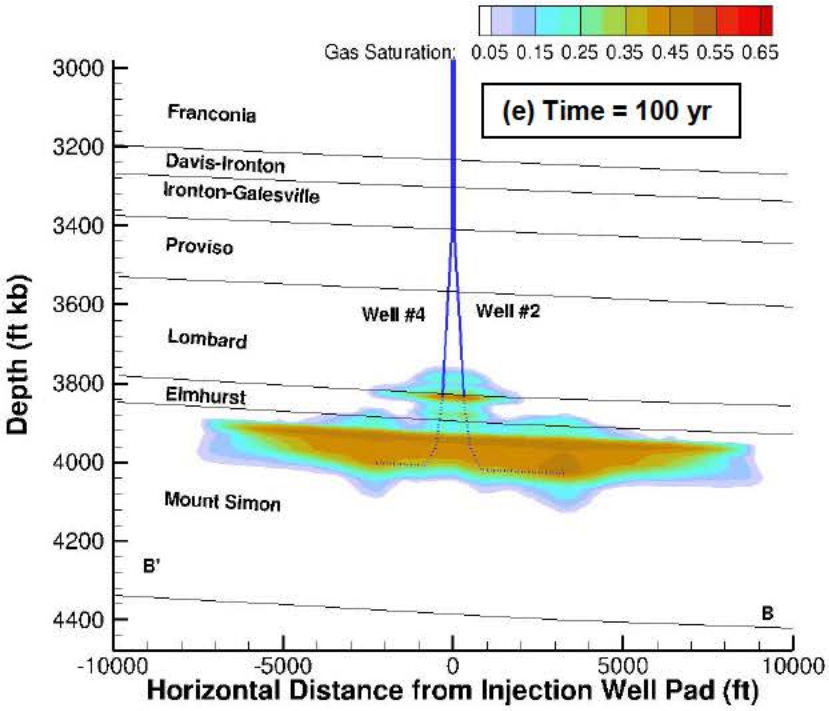

Figure 3.23. (contd)

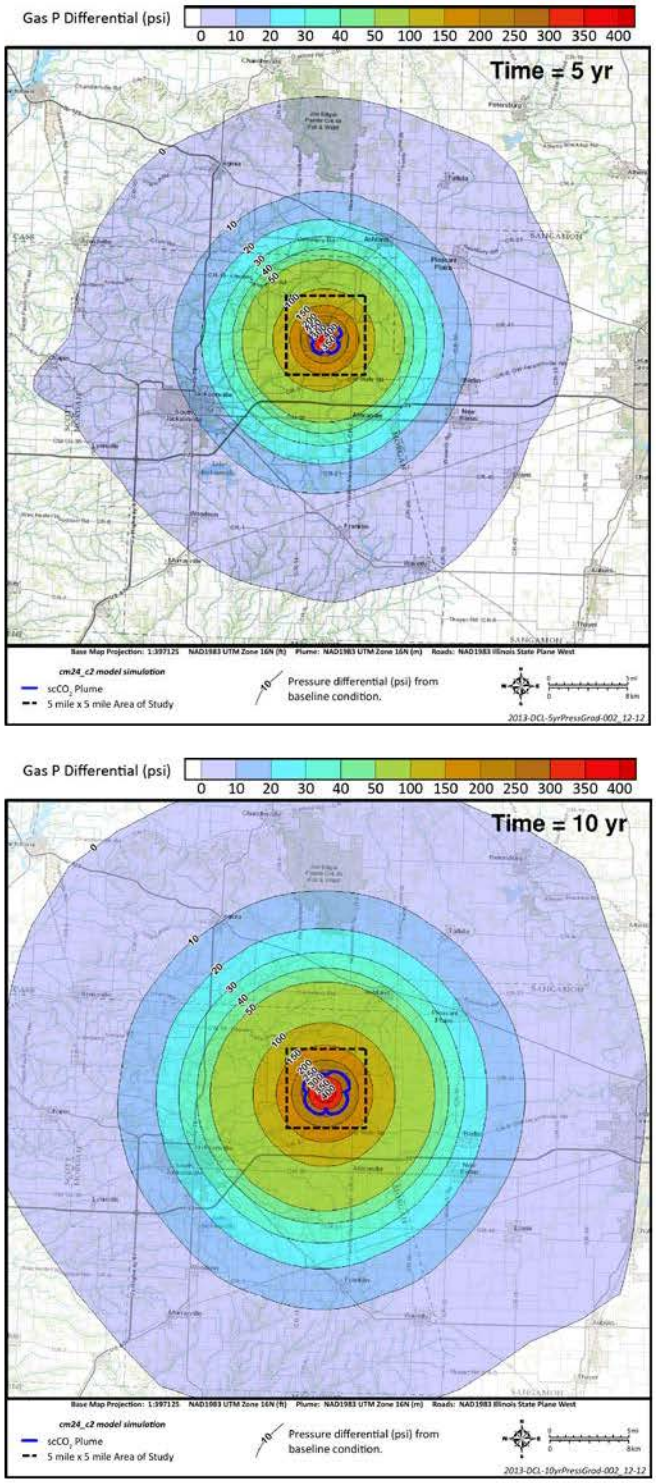

Figure 3.24. Pressure differentials from baseline condition and plume boundary at selected times (i.e., 5, 10, 20, 70, and 100 years). The plume area at 20 years is 6.35 mi^2, which is 1.7% less than the maximum plume extent at 22 years (6.46 mi^2). Twenty-five years after the end of injection (year 45), pressure differentials at the injection well location declines by 90%.

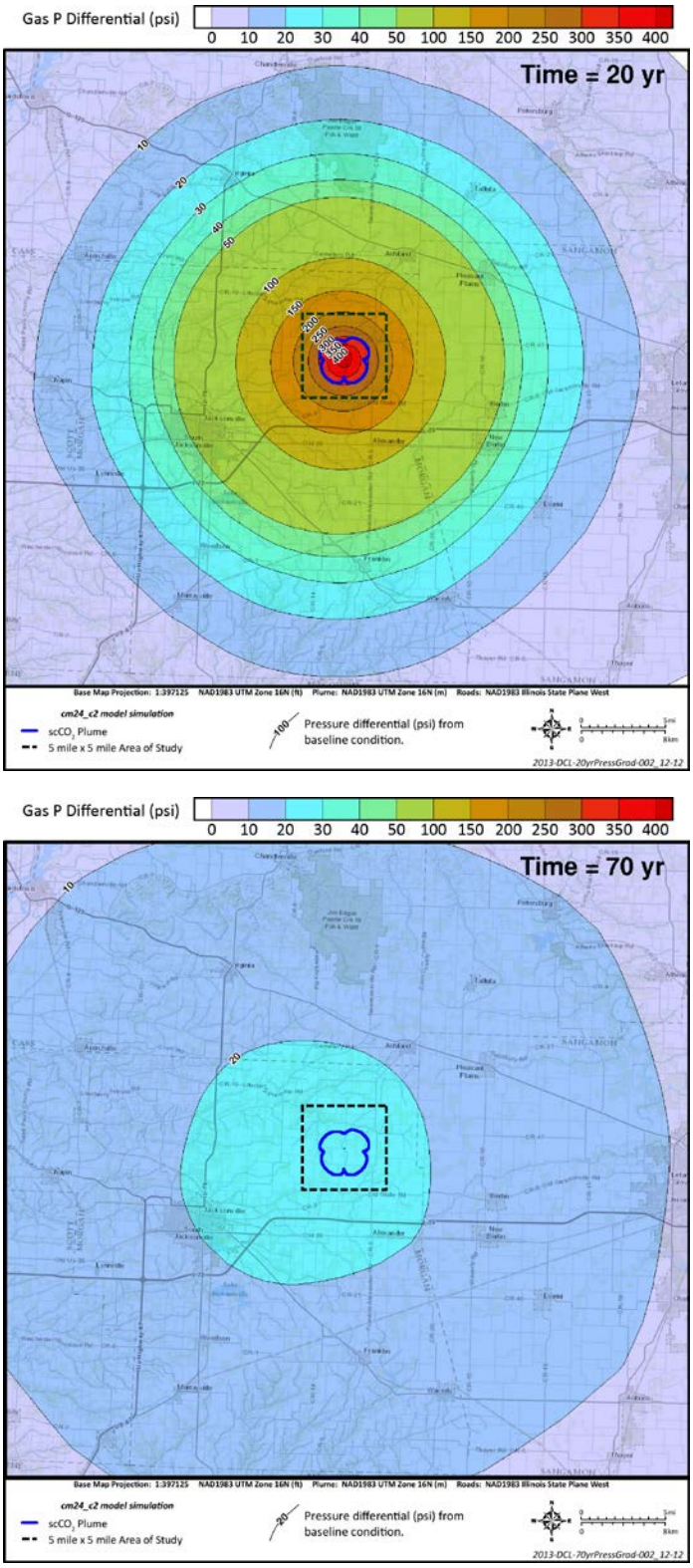

Figure 3.24. (contd)

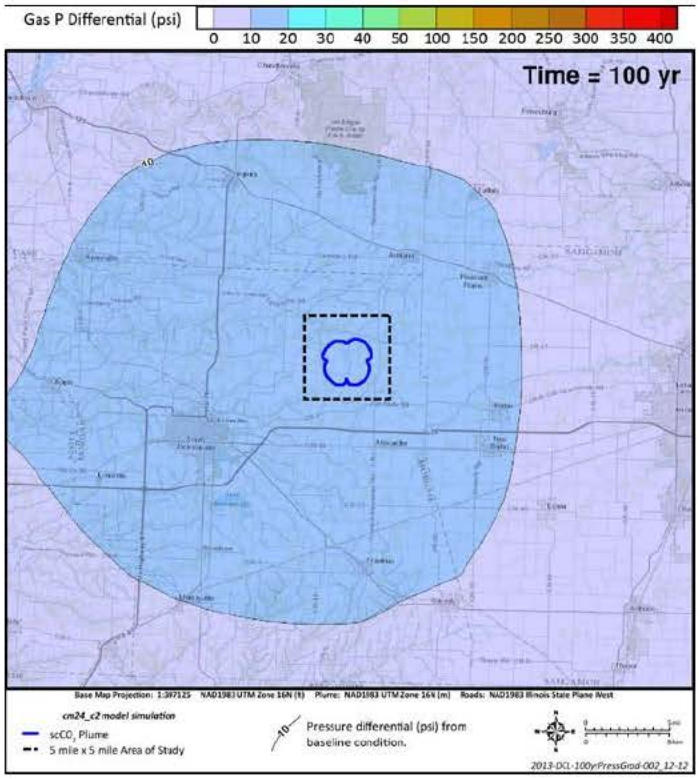

Figure 3.24. (contd)

Appendix D

RAI 11-14-2013_011
&
RAI11-14-2013_012

Additional Information Regarding

Parameter Sensitivity and Uncertainty

For the model sensitivity simulations, the probability distribution of each factor was assumed to be uniform within its uncertainty range (from minimum to maximum as given in Table 3.12 of the permit application). Samples of parameters within the uncertainty range were generated from the distributions to explore the impacts of the combinations of these factors on CO_2 transport. Traditional Monte Carlo (MC) sampling tends to produce many gaps and clumps, which may result in missing and/or duplicated numerical simulations. Consequently, to achieve stable results, often a large number of simulations (e.g., hundreds to even thousands) are required. The Quasi-Monte Carlo (QMC) sampling approach is an improved MC approach in which the parameter sequence is more evenly distributed in the multi-dimensional parameter space. It has advantages over the MC approach in that it can significantly improve the sampling efficiency and effectiveness, requiring many fewer numerical simulations to achieve stable results for quantifying sensitivity and uncertainty (Caflisch 1998; Wang and Sloan 2008; Hou et al. 2012). Therefore, the QMC approach is particularly applicable to computationally demanding numerical simulations and was used for this investigation.

The parameters that were considered in the sensitivity study were porosity, permeability, and fracture gradient. Their uncertainty ranges are given in Table 3.12 of the permit application. The three-dimensional parameter space was explored and the developed relationships and output statistics converged with 32 QMC parameter sets (which corresponds to 32 numerical simulations using STOMP). The resulting set of scaling factors was applied to the porosity and permeability values for all model layers and to the fracture gradient (0.585 psi/ft.). All layers were scaled by the same factor. In other words, when porosity or permeability is varied by a specified scaling factor, the corresponding parameter for all 51 layers is varied by the same factor. Therefore, we have provided a table (Table 1) of the scaling factors that were applied to the values listed in Table 3.8 of the permit application and to the fracture gradient. As an example, for case 1 in the table below, all 51 porosity values were varied by a factor of 1.2439, all 51 permeability values were varied by a factor of 1.1327, and the fracture gradient was varied by a factor of 0.9262 (resulting in an assigned value of 0.5418 [0.9262×0.585 psi/ft]).

References

Caflisch, R.E. 1998. Monte Carlo and quasi-Monte Carlo methods. *Acta Numerica* 7:1–49.

Hou, Z., M. Huang, L.R. Leung, G. Lin, and D.M. Ricciuto. 2012. Sensitivity of surface flux simulations to hydrologic parameters based on an uncertainty quantification framework applied to the Community Land Model. *Journal of Geophysical Research* 117, D15108.

Wang, X.Q., and I.H. Sloan. 2008. Low discrepancy sequences in high dimensions: How well are their projections distributed? *Journal of Computational and Applied Mathematics* 213:366–386.

Table 1. The scaling factors for porosity, permeability, and the fracture gradient.

Case	Porosity	Permeability	Fracture
1	1.2439	1.1327	0.9262
2	0.7521	0.9805	1.0086
3	0.9187	1.1471	1.0819
4	1.0854	0.8138	0.9352
5	0.8076	1.2027	0.8863
6	0.9743	0.8694	0.9597
7	1.1410	1.0360	1.0330
8	0.8632	0.7582	1.0575
9	1.0299	0.9249	0.9108
10	1.1965	1.0916	0.9841
11	0.7706	1.1101	1.0412
12	0.9373	0.7768	0.8945
13	1.1039	0.9434	0.9678
14	0.8262	0.8323	0.9923
15	0.9928	0.9990	1.0656
16	1.1595	1.1657	0.9189
17	0.8817	1.0546	0.9434
18	1.0484	1.2212	1.0167
19	1.2150	0.8879	1.0900
20	0.7891	0.9064	0.9271
21	0.9558	1.0731	1.0004
22	1.1225	1.2397	1.0738
23	0.8447	0.9620	1.0982
24	1.0113	1.1286	0.9515
25	1.1780	0.7953	1.0248
26	0.9002	1.1842	0.9760
27	1.0669	0.8508	1.0493
28	1.2336	1.0175	0.9026
29	0.7582	1.1533	0.9298
30	0.9249	0.8200	1.0031
31	1.0916	0.9867	1.0765
32	0.8138	0.8755	1.0276

Appendix E

RAI 14-11-2013_015

Additional Information Regarding

Rocks Properties

(Relative Horizontal Permeability)

Additional permeability corrections beyond the Klinkenberg correction were not applied. The K-Klinkenberg values were computed from K-air values, measured by Core Laboratories using an unsteady-state method, using the Klinkenberg Correction Factor (KCF). The KCF values were obtained for each sample using a standard procedure (Jones 1972). For some tight rocks it has been shown that the KCF may not be sufficient and that larger correction factors, such as the Knudsen correction factor, might be needed. The determination of whether a standard Klinkenberg can be used is typically based on the values of the Knudsen number, Kn (Kn = λ/r where λ is the molecular free path and r is characteristic length such as pore radius). For Knudsen numbers below ~2, differences between the KCF and the Knudsen correction factor are relatively small and additional permeability corrections are typically not needed (e.g., Ziarani and Aguilera 2012).

In Figure 1 (below), the computed KCF values are plotted against K-Klinkenberg for all analyzed samples. The plots show that for the tighter rocks (K-Klinkenberg < 0.01 mD), the KCF are always less than 10. Based on literature analyses (e.g., Civan 2010; Ziarani and Aguilera 2012), KCF values less than 10 indicate that the tighter samples are, in terms of the Knudsen flow regime, located in the lower end of the transition flow zone where 0.1 < Kn < 10. To confirm this observation, Kn values are computed using Eq. D1 for λ and Eq 17 for r in Ziarani and Aguilera (2012) and plotted in Figure 2 vs. K-Klinkenberg. The plot shows that for the tighter cores, Kn < 2. For these Kn values, the Knudsen correction factor may be up to 10% to 20% larger than the KCF. However, given the inherent uncertainties of unsteady-state permeability measurements in the < 0.01 mD range (Rushing et al. 2004), the slightly larger correction factor would result in permeability values within the experiment measurement error.

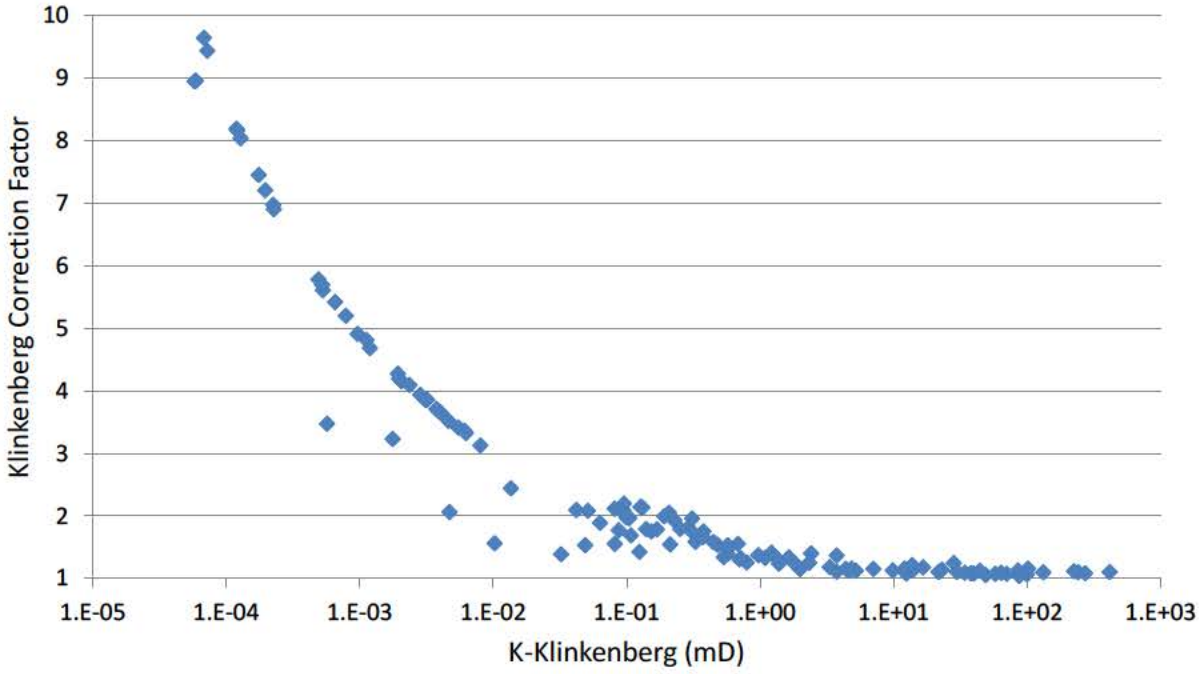

Figure 1. Klinkenberg correction factor as a function of K-Klinkenberg for all analyzed FutureGen core plugs.

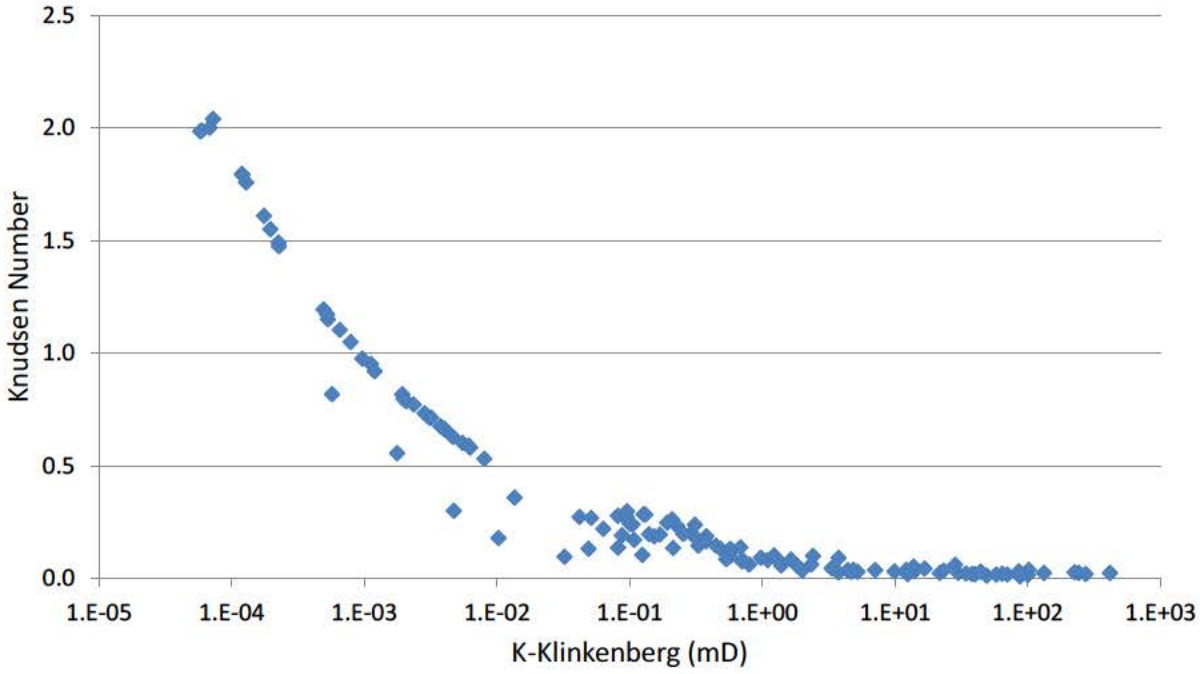

Figure 2. Computed Knudsen number as a function of K-Klinkenberg for all analyzed FutureGen core plugs.

References

Civan, F. 2010. Effective correlation of apparent gas permeability in tight porous media. *Transport in Porous Media* 82(2): 375-384.

Jones, S.C. 1972. A rapid accurate unsteady-state Klinkenberg permeameter. *Society of Petroleum Engineers Journal* 12(5):383–397.

Rushing, J.A., K.E. Newsham, P.M. Lasswell, and T.A. Blasingame. 2004. Klinkenberg-corrected permeability measurements in tight gas sands: Steady-state versus unsteady-state techniques. SPE Annual Technical Conference and Exhibition, 26-29 September 2004Houston, Texas. SPE 89867.

Ziarani, A.S., and R. Aguilera. 2012. Knudsen's permeability correction for tight porous media. *Transport in Porous Media* 91:239–260.

Appendix F

RAI 14-11-2013_018

Additional Information Regarding

Area of Review Pressure Front Delineation

(Critical Pressure Calculation)

As discussed in Birkholzer et al. (2011), a static critical threshold pressure determination for brine flow up an open conduit or damaged borehole (e.g., substandard well completion, deteriorating seal in abandoned well, near borehole drilling-related formation damage) may not be applicable for cases where permeable units exist between the injection reservoir and lowermost underground source of drinking water (USDW) because the open conduit approach doesn't account for lateral flow outside the conduit or casing and into these permeable zones. The effective permeability of an abandoned well or damaged zone surrounding a borehole would be smaller than flow in an unplugged well casing (i.e., open conduit) and permit brine to flow into intervening permeable formations (i.e., thief zones). At the FutureGen site there are many potential thief zones between the injection reservoir and the lowermost USDW, including 1) the Ironton Sandstone, 2) the Potosi Dolomite (which was identified as a very challenging lost-circulation zone during FGA#1 drilling activities, indicating extremely high-permeability conditions), and 3) the New Richmond Sandstone.

Birkholzer et al. (2011b) stated that a model is required to analyze these dynamic and transient impacts.

Objective and Approach

The objective of the analyses described below is to assess the potential of brine intrusion in the lowermost USDW. This calculation must consider the potential for brine migration along previously abandoned or poorly constructed wells that penetrate the caprock, driven by the reservoir pressure increases associated with supercritical carbon dioxide ($scCO_2$) injection. As noted by many authors and shown in results from our modeling, the extent of the pressure increase during $scCO_2$ injection is larger than the extent of the $scCO_2$ plume.

There are four penetrations that reach the Mount Simon within a radius of 35 miles (Figures 2.3 and 2.4 in the Supporting Documentation of the UIC permit applications). The nearest one is located at the Waverly field, 16 miles from the injection well. At this point, the maximum simulated pressure differential is 28 psi at 30 years after the beginning of the injection (Figure 3.24, in Appendix C, RAI# 11-14-2013_009) and a range of scenarios will be evaluated using the analytical model of Cihan et al. (2011).

Model Description, Assumptions, and Parameters

The analytic model used for this analysis was developed by Cihan et al. (2011) with additional examples of its use in Cihan et al. (2013). Pacific Northwest national Laboratory has obtained the source code, executable, and sample problems from the authors at Lawrence Berkeley National Laboratory. This model is for single-phase, isothermal fluid flow for focused leakage around wells and/or diffuse leakage through aquitards in a multilayered aquifer system from the transient pressure field created during reservoir injection. The model requires specification of the permeability, specific storage, and unit thickness for the reservoir, aquifers, and aquitards. It also needs borehole radii and effective permeabilities for the damaged zone around the borehole for each segment it passes through the aquifers/aquitards. The model does not account for brine density differences, but the results would be conservative because the volume of freshwater leakage calculated for each permeable unit would be greater than the higher density fluid in the reservoir at the FutureGen site.

Site data are limited for the upper layers (Ironton to St. Peter) at the FutureGen site because the focus of the detailed characterization of the first characterization borehole (FGA#1) was on the reservoir and caprock. Detailed characterization of the upper layers is planned for the next drilling campaign. Some sidewall core permeability measurements of these upper layers will be used along with values published for these units in the region or conservative estimates (i.e., using lower ranges of permeability estimates for the aquifers).

Effective permeability estimates for the damaged zone around a borehole will be based on published ranges of groupings of wells with different leakage potential (low, medium, high, extreme) as reported in Table 2 of Celia et al. (2011), which used the categories defined by Watson and Bachu (2008). Celia et al. (2011) used a stochastic modeling study with a large number of realizations for wells in the Wabamun Lake area of Alberta, Canada. Data from Crow et al. (2010) were also used by Celia et al. (2011) to develop these effective permeability estimates, which also highlighted the few measurements available. The high end of the high and extreme groupings will be investigated in this modeling effort. Single values of effective permeability around the borehole will be assigned for all the aquifer/aquitard segments, which provide conservative results based on Celia et al. (2011) analysis because using a range of permeabilities for a borehole through multiple layers would limit the fluxes based on the lower permeability values assigned.

The results of this analysis would be the volume of fluids leaked over time from the reservoir into each of the overlying aquifers (including the St. Peter, the lowermost USDW) for the two well distances (2 km and 26 km) using conservative estimates for the site parameters and the borehole effective permeabilities as discussed above.

A letter report will be provided in January 2014 describing the model, input parameters, and results of this analysis.

References

Birkholzer, J.T., J.P. Nicot, C.M. Oldenburg, Q. Zhou, S. Kraemer, and K.W. Bandilla. 2011. Brine Flow up a Borehole Caused by Pressure Perturbation from CO_2 Storage: Static and Dynamic Evaluations. *International Journal of Greenhouse Gas Control* 5(4):850–861.

Celia, M.A., J.M. Nordbotten, B. Court, M. Dobossy, and S. Bachu. 2011. Field-scale Application of a Semi-Analytical Model for Estimation of CO_2 and Brine Leakage Along Old Wells. *International Journal of Greenhouse Gas Control* 5:257–269.

Cihan A., Q. Zhou, and J-T. Birkholzer. 2011. Analytical solutions for pressure perturbation and fluid leakage through aquitards and wells in multilayered-aquifer systems. *Water Resources Research* 47.

Cihan A., J-T. Birkholzer, and Q. Zhou. 2013. Pressure Buildup and Brine Migration During CO_2 Storage in Multilayered Aquifers. *Groundwater* 51(2).

Crow, W., J.W. Carey, S. Gasda, B. Williams, and M.A. Celia. 2010. Wellbore integrity analysis of a natural CO_2 producer. International Journal of Greenhouse Gas Control 4:186–197.

Watson, T. L., and S. Bachu. 2008. Identification of Wells with High CO_2-Leakage Potential in Mature Oil Fields Developed for CO_2-Enhanced Oil Recovery. Paper SPE 11294, SPE Improved Oil Recovery Symposium, Tulsa, Oklahoma.

Appendix G

RAI14-11-2013_019

Additional Information Regarding

Area of Review Pressure Front Delineation

(Pressure Differential / Simulation Time)

Details of Pressure Front Calculation:

Determining the pressure front ($P_{i,f}$) was calculated from Equation 4 of the EPA Draft Guidance (2011, page 35):

$$P_{i,f} = P_u \cdot \frac{\rho_i}{\rho_u} + \rho_i \cdot g \cdot (z_u - z_i)$$

where:

P_i, P_u = pressure (pre-injection) in injection zone and USDW (respectively), Pa
ρ_i, ρ_u = fluid density in injection zone and USDW (respectively), kg/m^3
z_i, z_u = elevation of injection zone and USDW (respectively), m
g = Acceleration of Gravity.

Glacial Aquifer		
Parameter	**Value**	**Notes**
Bottom Elevation (z_u)	149 m (489 ft MSL)	
Pre-Injection Pressure (P_u)	364,305 Pa (52.838 psi)	
Water Density (ρ_u)	1,000 kg/m^3	Freshwater density

Injection Zone – Mt. Simon / Top of Elmhurst		
Parameter	**Value**	**Notes**
Elevation (z_i)	-981 m (-3219 ft MSL)	
Pre-Injection Pressure (P_i)	11,608,700 Pa (1683.7 psi)	Extrapolated from MDT and packer measurements in Mt. Simon (see Figure 2.29 in UIC permit).
Brine Density (ρ_i)	1,033 kg/m^3	Online water density calculator: www.csgnetwork.com/water_density_calculator.html P = 1683.70 psi, T=96.155 F, TDS = 47,000 ppm (47 PSU)

Reference

EPA (U.S. Environmental Protection Agency). 2011. *Draft Underground Injection Control (UIC) Program Class VI Well Area of Review Evaluation and Corrective Action Guidance for Owners and Operators*. EPA 816-D-10-007, EPA Office of Water, Washington, D.C.